Supplementary Information:

Patient-Derived Models Recapitulate Heterogeneity of Molecular Signatures and Drug Response in Pediatric High-Grade Glioma

Chen He*[1], Ke Xu*[2,3], Xiaoyan Zhu*[1], Paige S. Dunphy*[1,4], Brian Gudenas[1], Wenwei Lin[5], Nathaniel Twarog[5], Laura D. Hover[1], Chang-Hyuk Kwon[1], Lawryn H. Kasper[1], Junyuan Zhang[1], Xiaoyu Li[6], James Dalton[6], Barbara Jonchere[7], Kimberly S. Mercer[7], Duane G. Currier[5], William Caufield[8], Yingzhe Wang[8], Jia Xie[5], Alberto Broniscer[9], Cynthia Wetmore[10], Santhosh A. Upadhyaya[4], Ibrahim Qaddoumi[4], Paul Klimo[11], Frederick Boop[11], Amar Gajjar[4], Jinghui Zhang[3], Brent A. Orr[6], Giles W. Robinson[4], Michelle Monje[12], Burgess B. Freeman[8], Martine F. Roussel[7], Paul A. Northcott[1], Taosheng Chen[5], Zoran Rankovic[5], Gang Wu[2,3], Jason Chiang[6#], Christopher L. Tinkle[13#], Anang A. Shelat[5#], and Suzanne J. Baker[1#]

Departments of [1] Developmental Neurobiology, [2] Center for Applied Bioinformatics, [3]Computational Biology, [4] Oncology, [5] Chemical Biology and Therapeutics, [6] Pathology, [7] Tumor Cell Biology, [8] Preclinical Pharmacokinetics Shared Resource St. Jude Children's Research Hospital, Memphis TN. 38105

[9] Division of Hematology-Oncology, Children's Hospital of Pittsburgh, Pittsburgh, PA
[10] Exelixis, Alameda, CA
[11] Department of Surgery, St. Jude Children's Research Hospital, Memphis TN. 38105
[12] Department of Neurology, Stanford University, Stanford, CA
[13] Department of Radiation Oncology, St. Jude Children's Research Hospital, Memphis TN. 38105

*Shared first authors contributed equally

#Shared corresponding authors
Suzanne.Baker@StJude.org
Anang.Shelat@StJude.org
Christopher.Tinkle@StJude.org
Jason.Chiang@StJude.org

Supplementary Figure 1: **Heatmap of large-scale copy number changes in patient tumors, PDOX, and cell lines.** Patient tumor and matched PDOX and cell lines are grouped together in columns. Abbreviated line numbers are listed across the top. Rows show large scale gain (red) or loss (blue) of chromosome arms indicated at right. Scored large-scale copy number changes encompassed more than 50% of a chromosome arm.

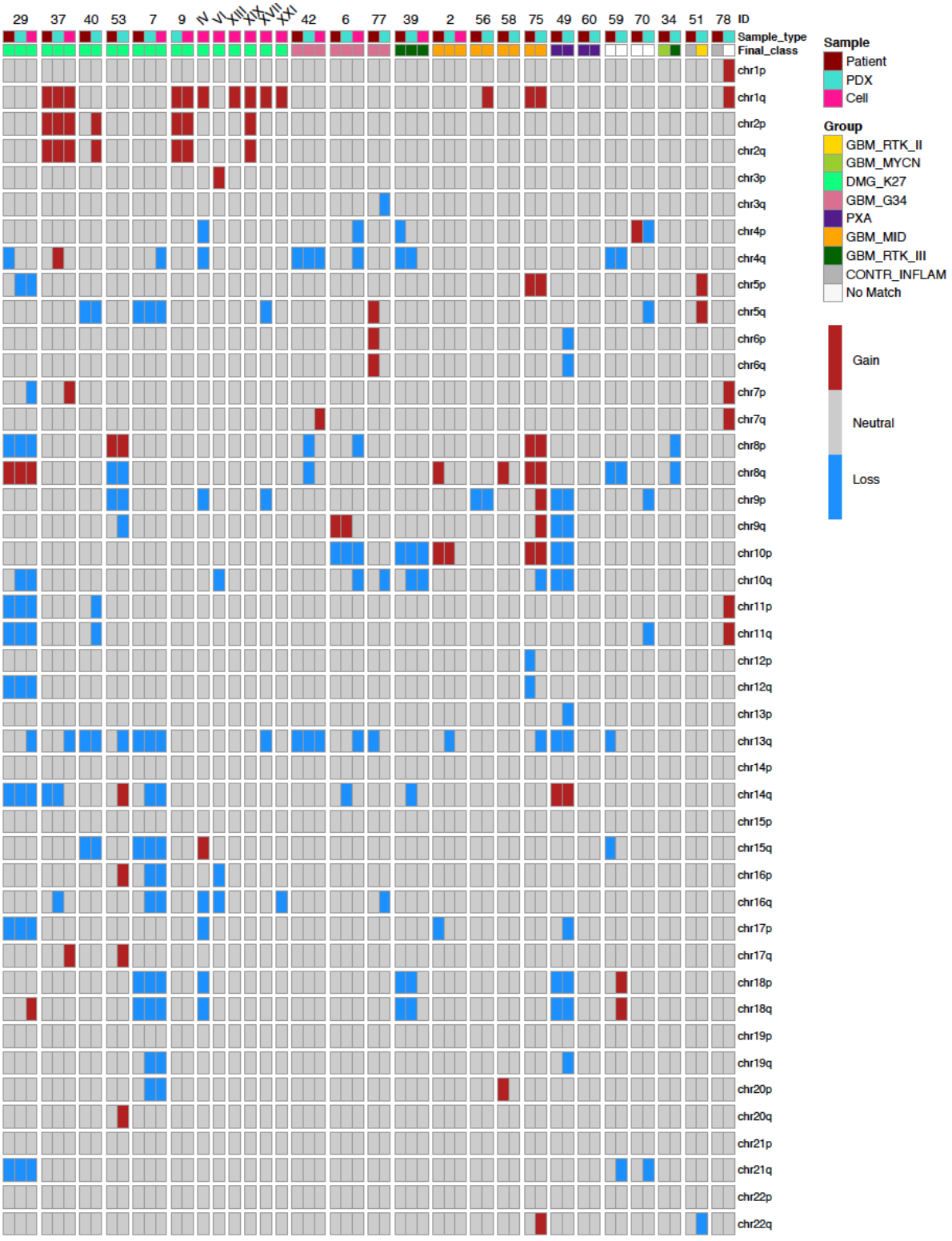

Supplementary Figure 2: **Extra-chromosomal DNA amplifications in PDOX models.** (a) WGS (top 3 tracks) and RNA-seq (lower 3 tracks) showed amplification and overexpression, respectively, of a TMEM165-PDGFRA fusion gene in SJ-HGGX75 patient tumor and matched PDOX compared to normal copy number and expression in SJ-HGGX70. The structural variant connecting the boundaries of the amplified segment was identified in WGS of SJ-HGGX75 patient tumor and matched PDOX. (b) TMEM165-PDGFRA fusion gene was identified from RNA-seq data using CICERO in SJ-HGGX75 patient tumor and matched PDOX. The resulting chimeric protein replaces the most N-terminal Ig-like domains of PDGFRα with 70 amino acids from the N-terminus of TMEM165. (c) Interphase fluorescence *in situ* hybridization of PDOX SJ-HGGX75 shows amplification of *PDGFRA* (red, 4q12; control, green, 4p12) in the form of double minutes in 100% of the 200 evaluable nuclei. (d) WGS (top 3 tracks) and RNA-seq (lower 2 tracks) showed *MYCN* amplification and overexpression, respectively, in the PDOX from SJ-DMGX40, but not the diagnostic tumor from which it was derived, or autopsy from the same patient. (e) Interphase fluorescence *in situ* hybridization of PDOX SJ-DMGX40 shows amplification of *MYCN* (red, 2p24; control, green, 2q35) in the form of double minutes in 100% of the 200 evaluable nuclei. Scale bar in c,e: 15 µm

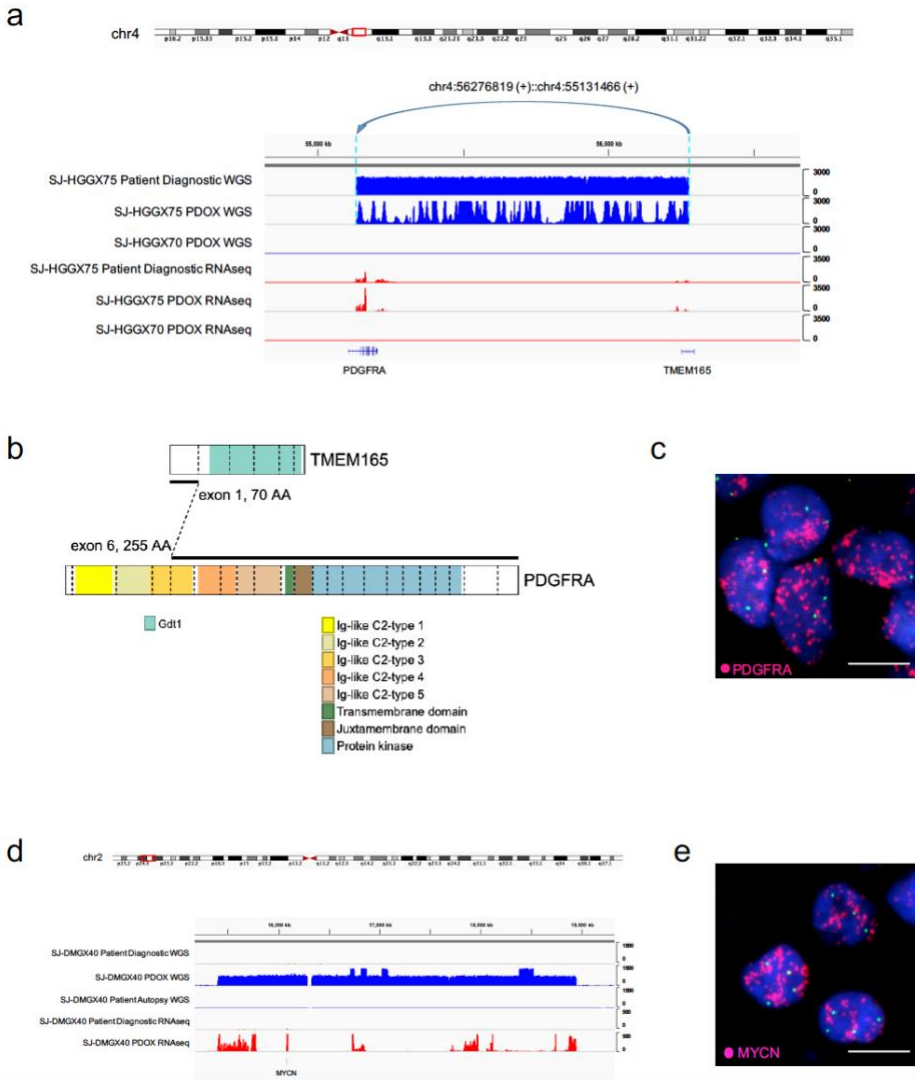

Supplementary Figure 3: Expression signatures of PDOX models recapitulate primary tumors from which they are derived. Pearson correlation coefficient of RNA-seq quantification (logCPM) between each PDOX sample and all 16 patient tumors that have matched PDOXs. The red dots represent the Pearson correlation coefficient between each PDOX sample and the matched patient tumor, black dots show correlation between each PDOX sample and other patient tumors. Genes include all mRNA genes except those identified as genes differentially expressed between all PDOX compared to patient tumors (Supplementary Data 3).

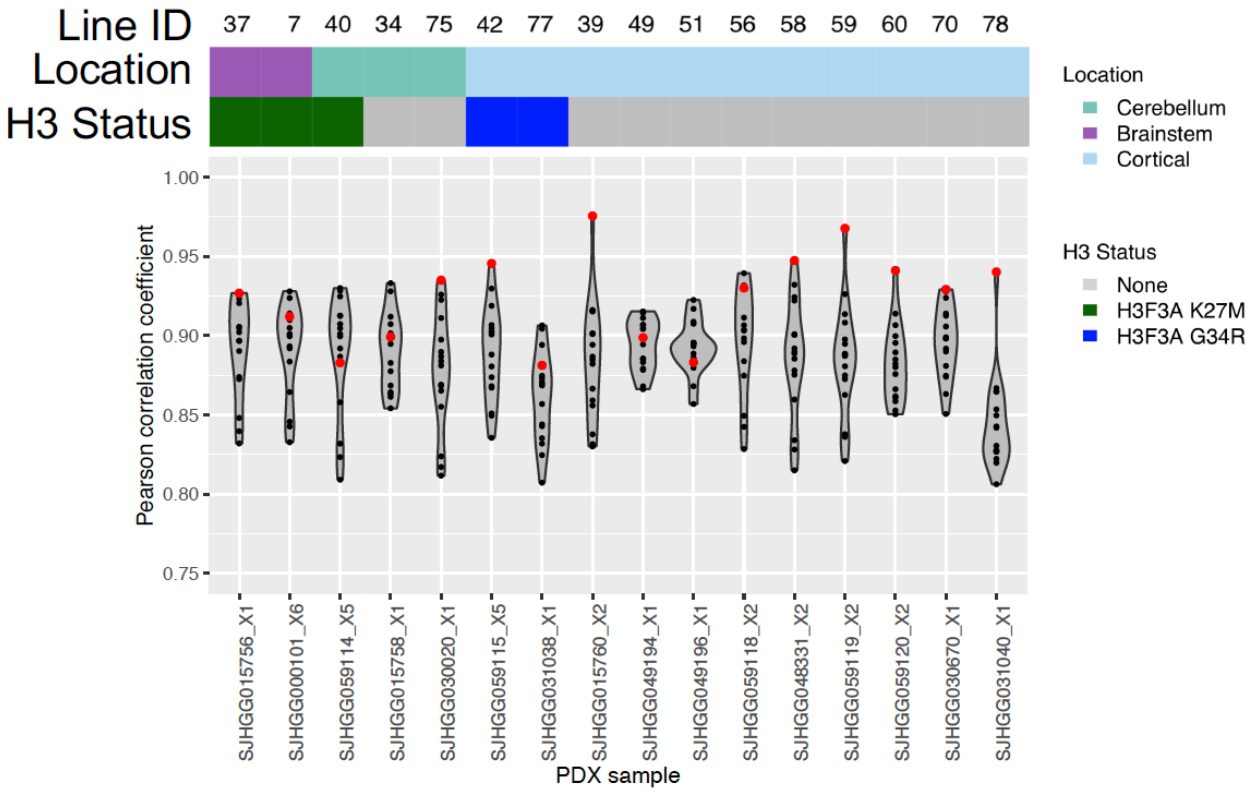

Supplementary Figure 4. Fidelity of expression signatures in PDOX models from different passages, and in cell lines compared with the PDOX from which they were derived. Scatterplot comparing expression (RNAseq, logCPM) in indicated PDOX and cell lines. $p<2.2x10^{-16}$

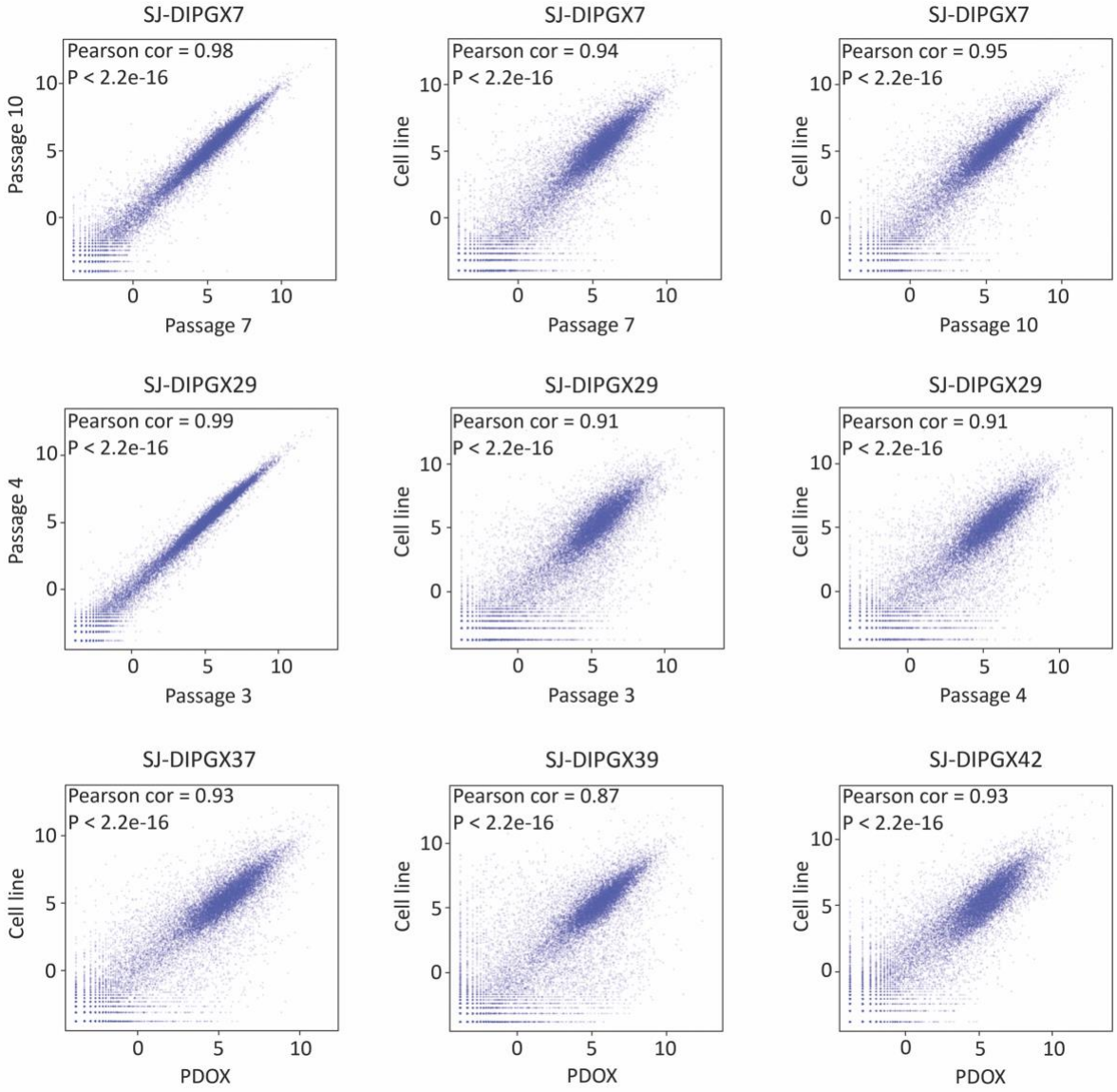

Supplementary Figure 5: Example summary of pHGG model characterization available through Pediatric Brain Tumor Portal. Summary data for PDOX line SJ-HGGX42 and associated samples is shown here as a representative example of data available for all 21 PDX models. PDF summaries for each model can be accessed and downloaded from the PBTP, and this information and multiple additional options for interactive exploration of data from this paper are available through the online portal.

Pediatric Brain Tumor Portal

Summary

Name: SJ-HGGX42
Sample ID: SJHGG059115
Disease: High-grade Glioma
Associated Acronyms: HGG, GBM
Histone H3 Status: H3.3 G34R

Clinical Information

Clinical Group: Cortical HGG
Pathologic Group: Glioblastoma
Grade: IV
Patient Sample Type: Diagnostic
Survival from Diagnosis: 12 months
Sex: Male
Patient Tumor Location: Cortical
Treatment History: Treatment Naive

Sample Information

PDOX Label: YFP-Luciferase
Cell Line Label: YFP-IRES-Luciferase
Mouse Survival (PDOX→PDOX): 5 months
Mouse Survival (cell culture→PDOX): 5 months
Material Available: PDOX, Cell line

Sequence Source and Oncoprint

Sample	Sample ID	WGS	WES	RNAseq	Methylation
Patient Germline	SJHGG059115_G1	N/A	N/A	N/A	N/A
Patient Tumor (Diagnostic)	SJHGG059115_D1	✓	✓	✓	✓
PDOX Tumor (Derived from Diagnostic)	SJHGG059115_X5	✓	✓	✓	✓
Cell line (Derived from PDOX)	SJHGG054830_C2	N/A	✓	✓	✓
PDOX Tumor (Derived from cell line)	SJHGG059115_X31	✓	✓	✓	✓
Patient Tumor (Autopsy)	SJHGG059115_A1	✓	✓	✓	✓

Table indicates sequencing performed (✓); WGS, whole genome sequencing; WES, whole exome sequencing; RNAseq, RNA sequencing; Methylation, BeadChip array profiling human DNA methylation; N/A, sequence not available.

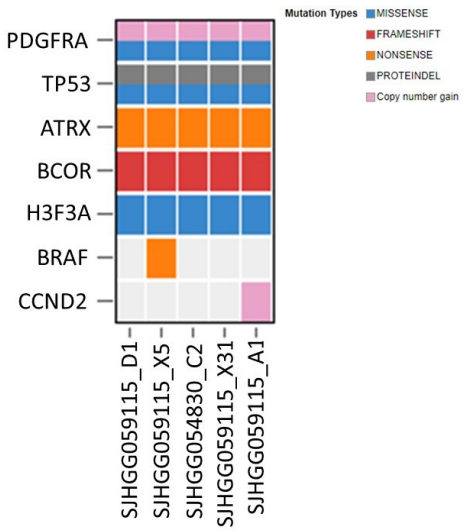

Oncoprint for pediatric high-grade glioma signature mutations in these samples.

Histology

H&E

Patient Tumor

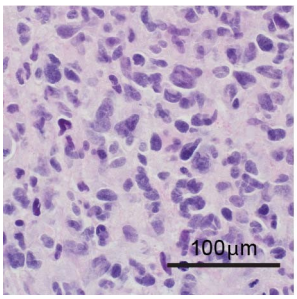

PDOX Tumor

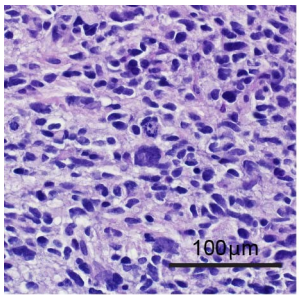

ATRX

Patient Tumor

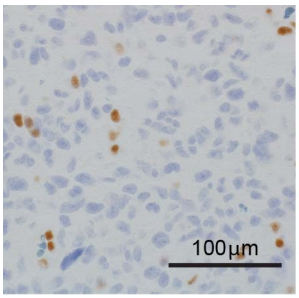

PDOX Tumor

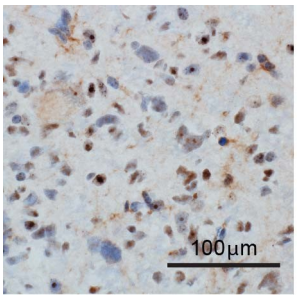

Mutation Status

ATRX

Sample	aa change
SJHGG059115_D1	S692*
SJHGG059115_X5	S692*
SJHGG054830_C2	S692*
SJHGG059115_X31	S692*
SJHGG059115_A1	S692*

BCOR

Sample	aa change
SJHGG059115_D1	S177fs
SJHGG059115_X5	S177fs
SJHGG054830_C2	S177fs
SJHGG059115_X5	S177fs
SJHGG059115_X5	S177fs

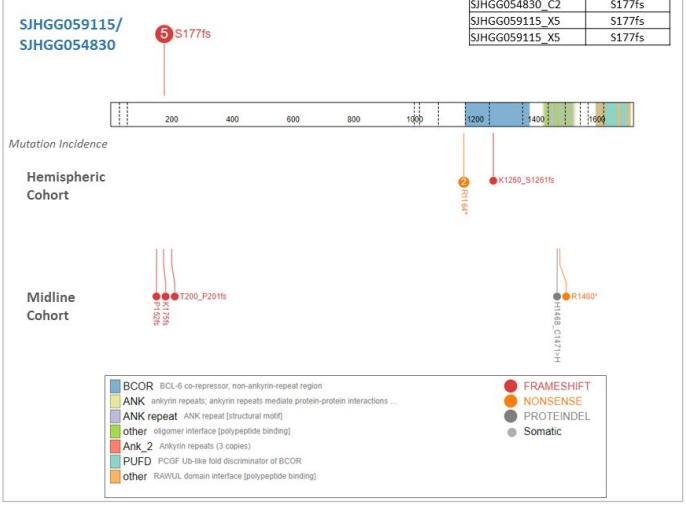

BRAF

Sample	aa change
SJHGG059115_D1	--
SJHGG059115_X5	S316*
SJHGG054830_C2	--
SJHGG059115_X31	--
SJHGG059115_A1	--

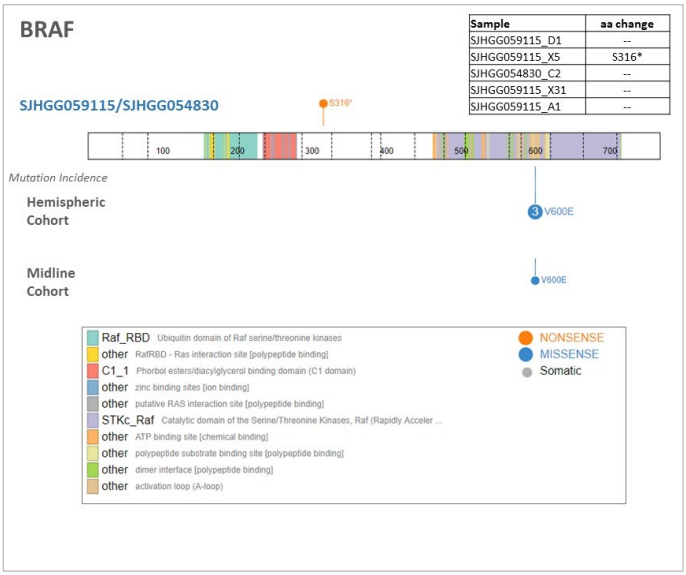

PDGFRA

Sample	aa change
SJHGG059115_D1	P343S
SJHGG059115_X5	P343S
SJHGG054830_C2	P343S
SJHGG059115_X31	P343S
SJHGG059115_A1	P343S

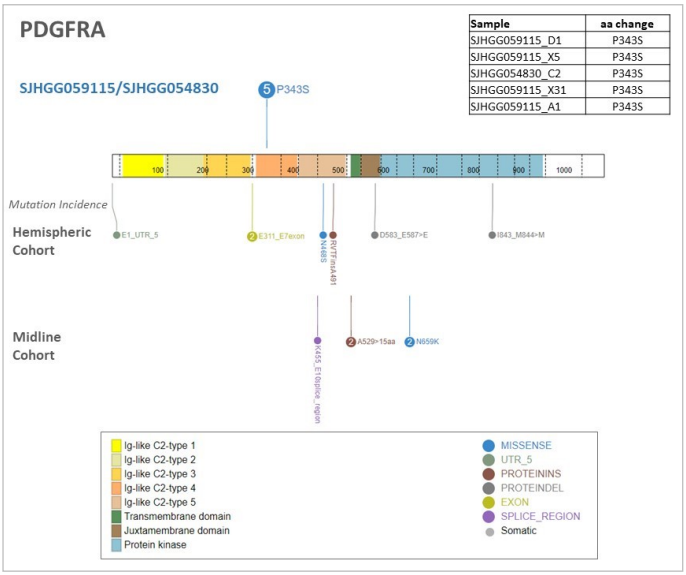

TP53

Sample	aa change
SJHGG059115_D1	L264_L265>L
SJHGG059115_D1	R248Q
SJHGG059115_X5	L264_L265>L
SJHGG059115_X5	R248Q
SJHGG054830_C2	L264_L265>L
SJHGG054830_C2	R248Q
SJHGG059115_X31	L264_L265>L
SJHGG059115_X31	R248Q
SJHGG059115_A1	L264_L265>L
SJHGG059115_A1	R248Q

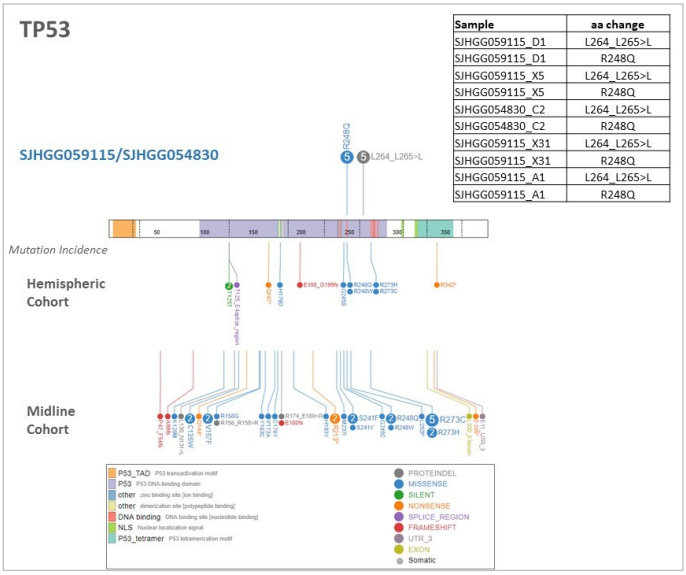

H3F3A

Sample	aa change
SJHGG059115_D1	G34R
SJHGG059115_X5	G34R
SJHGG054830_C2	G34R
SJHGG059115_X31	G34R
SJHGG059115_A1	G34R

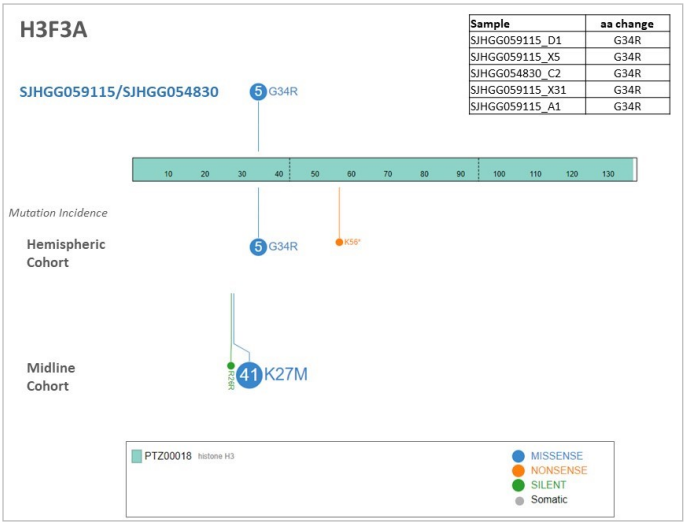

Figure legend, see page 3

Mutation Status figure legend:

Protein paint diagrams show schematic of protein with functional domains shown in legend box. Mutations associated with samples for this line are shown above the protein diagram. Mutations in cohort of 127 pediatric HGGs separated as hemispheric and midline tumors from [1] are shown below. Number of samples with the specific mutation are listed in the circle marking the mutated residue.

Copy Number Variation

Patient Tumor
SJHGG059115_D

PDOX Tumor
SJHGG059115_X

Cell line*
SJHGG054830_C

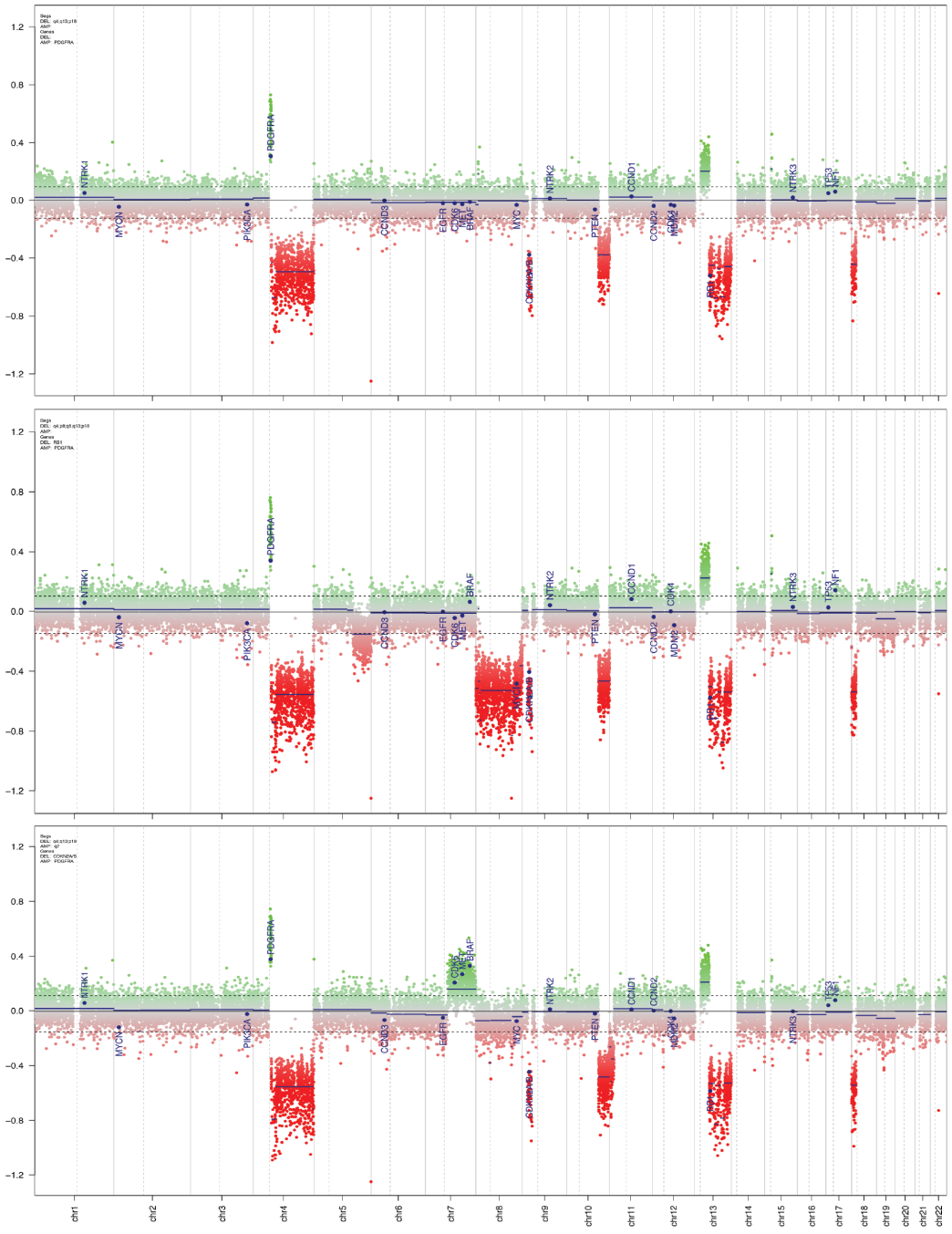

*Cell line derived from PDOX

DNA copy number variation analysis was performed from methylation array data using Conumee [2]. The Y axis shows the log2 copy number ratio of the tumor sample compared to a panel of normal reference brain tissues. Copy number ratios are plotted across chromosomes with the dotted vertical lines representing centromeres. Chromosomal gains or losses are detected as significant positive or negative deviations from genomic baseline. Brain tumor relevant gene regions are highlighted for easier assessment of chromosomal or focal alterations.

Brain Tumor Methylation Classification

t-SNE plot showing glioma subgroups based on DNA methylation profiling. Patient tumors (circles), PDOX (squares) and cell lines (diamonds) reported here are outlined in black and reference samples from [3] shown without black outline. Enlarged area shows the methylation class cluster for this sample, and circled samples show the matched samples for this PDOX.

Sample	Methylation Class
Patient Tumor	glioblastoma, IDH wildtype, H3.3 G34 mutant
PDOX Tumor	glioblastoma, IDH wildtype, H3.3 G34 mutant
Cell Line (derived from PDOX)	glioblastoma, IDH wildtype, H3.3 G34 mutant

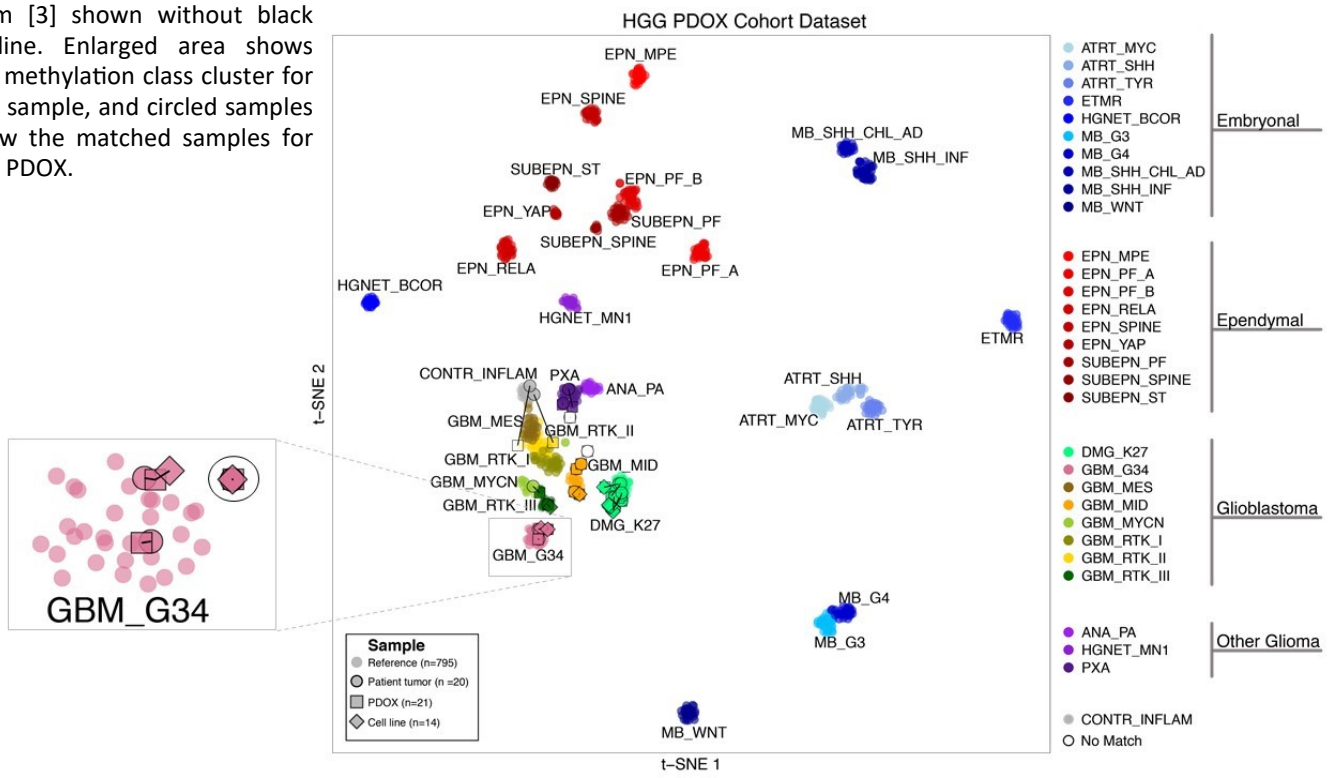

Short Tandem Repeat (STR) DNA Typing

Marker	Allele 1	Allele 2
Amelogenin	X	Y
CSF1PO	10	11
D13S317	13	
D16S539	9	11
D18S51	12	18
D21S11	29	30
D3S1358	14	15
D5S818	13	
D7S820	11	12
D8S1179	13	
THO1	6	9.3
TPOX	9	11
vWA	17	18

DNA fingerprint from Promega PowerPlex 16 STR assay.

References

1. Wu, G. *et al. Nat. Gen.* **46**, 444-450 (2014).
2. Hovestadt, V. & Zapatka, M. Conumee: enhanced copy-number variation analysis using Illumina methylation arrays. v.1.4.2 R package v.0.99.4 http://www.bioconductor.org/packages/release/bioc/html/conumee.html (2015) .
3. Capper, D. *et al. Nature.* **555**, 469-474 (2018).

Supplementary Figure 6: DIPG cells grown as tumorspheres or adherent cultures on Geltrex basement membrane matrix respond similarly when tested with 53 drugs representing a range of different mechanisms of action.

Scatterplot of AUCs testing dose-response for 53 compounds in SJ-DIPGX7c grown under adherent vs neurosphere conditions. The Pearson correlation is 0.994. Black line has slope = 1.

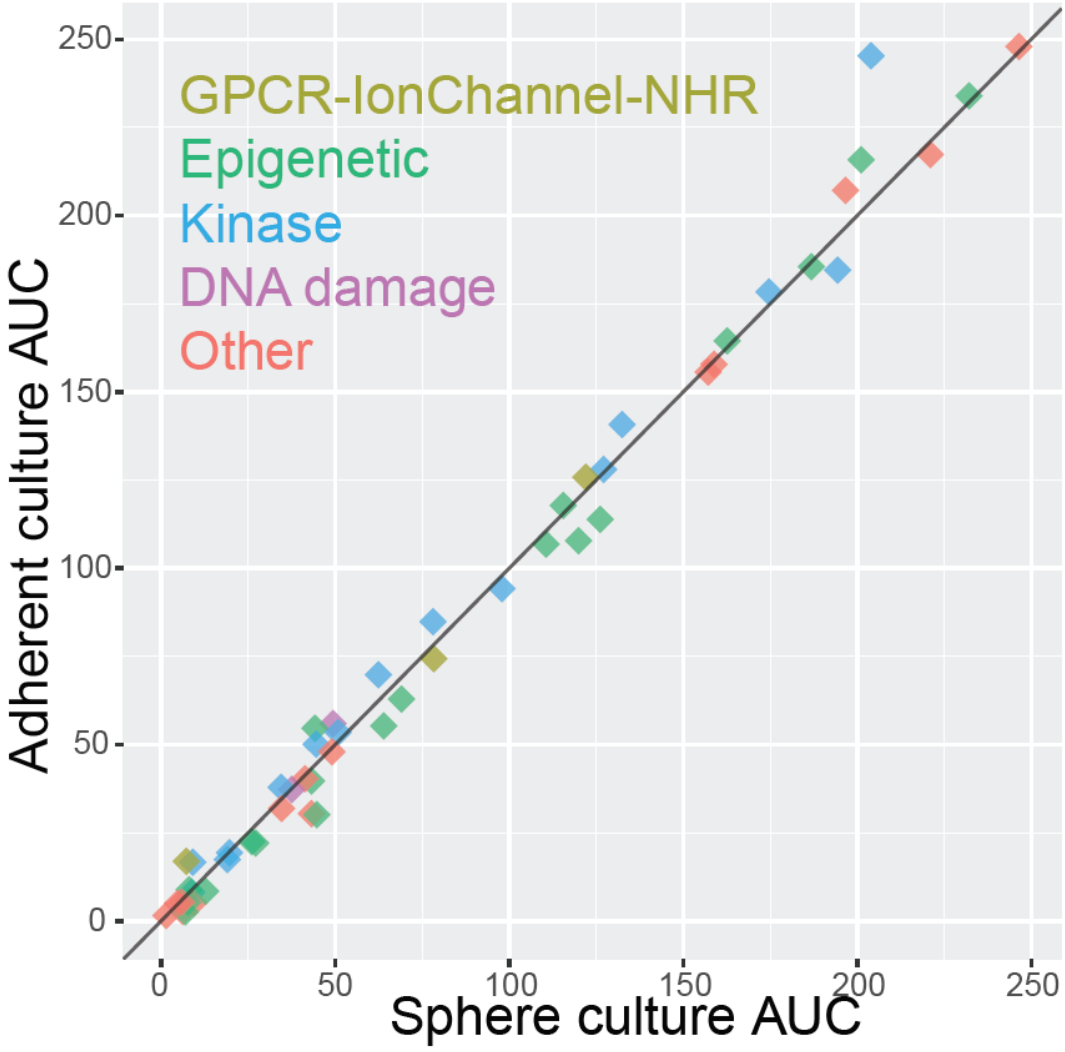

Supplementary Figure 7: Z prime values for drug screening in 16 cell lines from 310 384-well assay plates. Scatterplot of Z prime values for each plate screened in this study color coded by cell lines assayed. A Z prime score between 0.5 and 1 indicates an excellent signal to noise ratio.

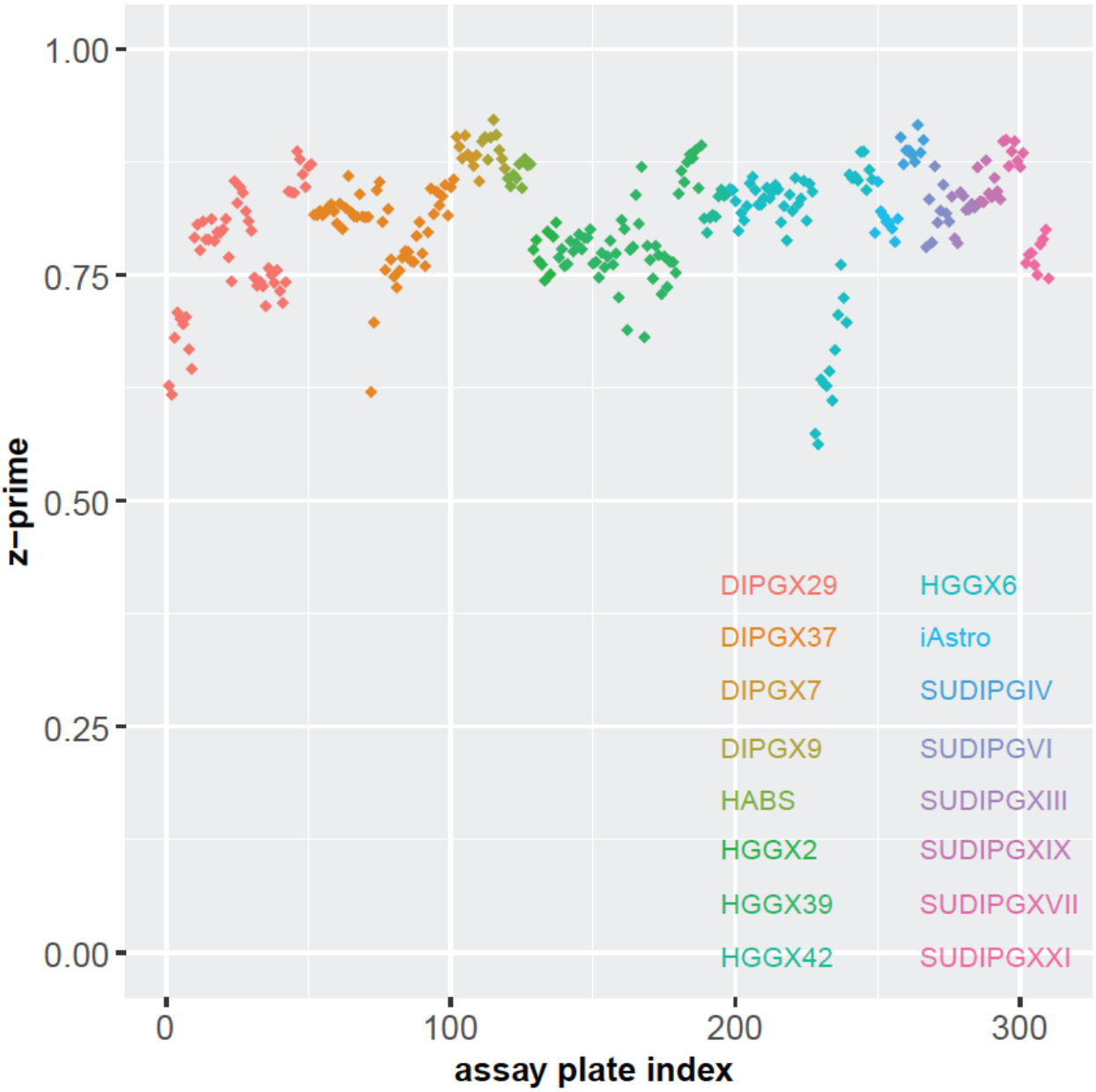

Supplementary Figure 8: Additional analysis of the screening results from 93 compounds across 14 pHGG models and two normal astrocyte lines. (a) Select dose-response curves for the drugs highlighted in Figure 6b. iAstro is depicted in black dashed lines, HABS in black solid lines, and pHGG models are colored gray or by histone mutation status where DIPGX37 is indicated. (b) Scatterplot of MAPK pathway activation score (MPAS) vs AUC for all 14 pHGG cell lines treated with trametinib. The Pearson correlation is -0.34. (c)Unsupervised hierarchical clustering of drug AUC z-scores for all compounds tested. Column and column labels are color coded by histone mutation status. Each row represents a single compound and is annotated by mechanism of action with color code shown above. The color code for histone mutation status is: H3-wt (red), H3.3 G34R (blue), H3.1 K27M (turquoise), and H3.3 K27M (green). Control cell lines (iAstro and HABS) are black.

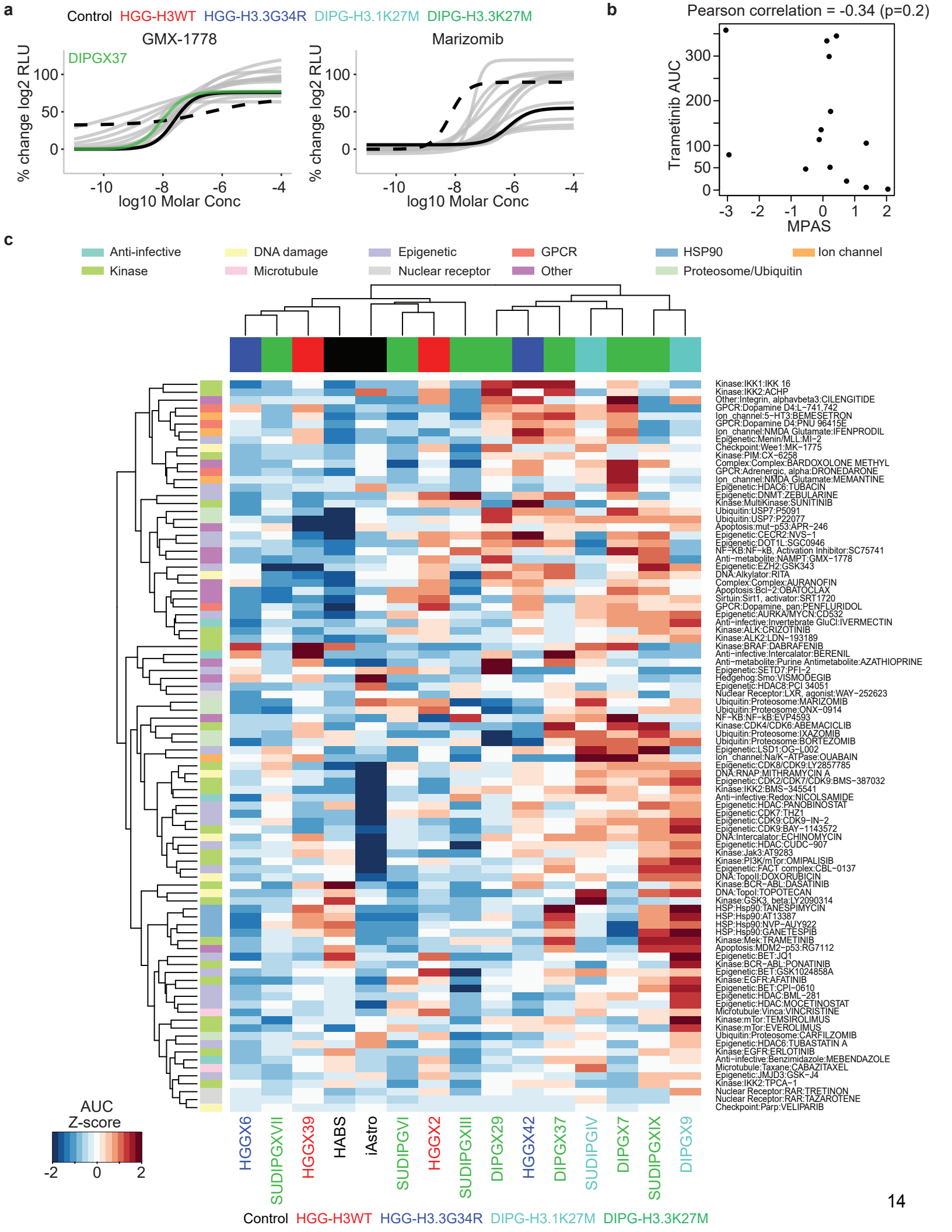
a
Control HGG-H3WT HGG-H3.3G34R DIPG-H3.1K27M DIPG-H3.3K27M
GMX-1778
DIPGX37
Marizomib
% change log2 RLU
log10 Molar Conc
b
Pearson correlation = -0.34 (p=0.2)
Trametinib AUC
MPAS
c
Anti-infective
DNA damage
Epigenetic
GPCR
HSP90
Ion channel
Kinase
Microtubule
Nuclear receptor
Other
Proteosome/Ubiquitin
AUC Z-score
HGGX6
SUDIPGXVII
HGGX39
HABS
iAstro
SUDIPGVI
HGGX2
SUDIPGXIII
DIPGX29
HGGX42
DIPGX37
SUDIPGIV
DIPGX7
SUDIPGXIX
DIPGX9
Control HGG-H3WT HGG-H3.3G34R DIPG-H3.1K27M DIPG-H3.3K27M
14

Supplementary Fig. 9: Pharmacodynamic analyses of mirdametinib and paxalisib show effective MEK and PI3K pathway inhibition in the brain

Western blots from a single pharmacodynamic experiment with the indicated antibodies to analyze lysates from: (a) SJ-DIPGX37 intracranial tumors in mice dosed with vehicle (veh, lanes 1-3), 25 mg/kg mirdametinib (mir, lanes 4-6), or 18 mg/kg paxalisib (pax, lanes 7-9) daily for 5 days, and tissue collected 2 hours after last dose. Antibodies are shown at the right. (b) Brain from CD1-nude mice treated with vehicle (lanes 1-3), 8 mg/kg pax (lanes 4-6), 12 mg/kg pax (lanes 7-9), 8 mg/kg pax + 14 mg/kg mir (lanes 10-12) and 12 mg/kg pax + 17 mg/kg mir (lanes 13-15). (c) Brain from CD1-nude mice treated with vehicle (lanes 1-3), 14 mg/kg mir (lanes 4-6), 17 mg/kg mir (lanes 7-9), 14 mg/kg mir + 8 mg/kg pax (lanes 10-12) and 17 mg/kg mir + 12 mg/kg pax (lanes 13-15). n=3 mice per treatment, with each lane containing lysate from one mouse.

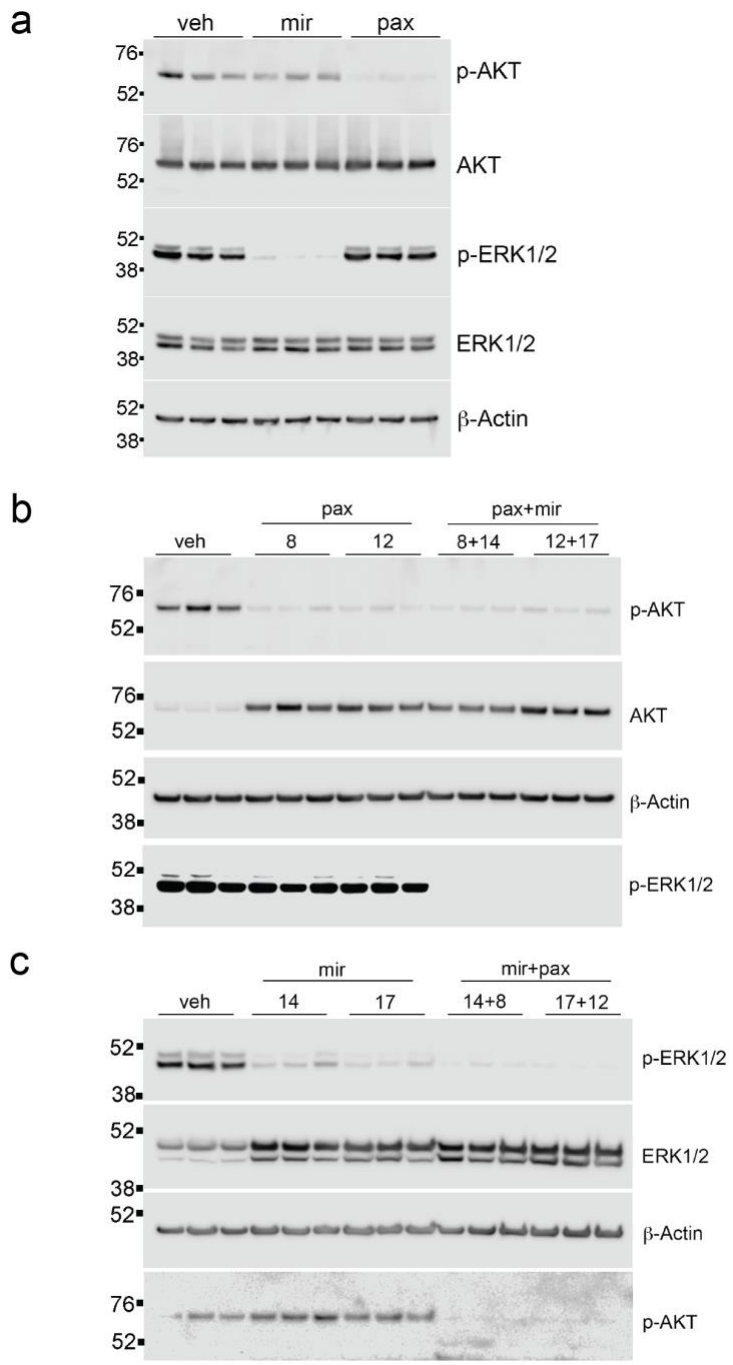

Supplementary Fig 10: Pharmacokinetic (PK) and pharmacodynamic analyses of Paxalisib and Mirdametinib show lack of appreciable plasma or brain PK drug interaction, high brain exposure, and effective pathway inhibition

a. Mirdametinib population mean and 90% prediction interval plasma concentration-time profiles alone (mir) and in combination with Paxalisib (mir+pax). A minor increase in Mirdametinib AUC (1.30-fold) was observed in combination.
b. Paxalisib population mean and 90% prediction interval plasma concentration-time profiles alone (pax) and in combination with Mirdametinib (pax+mir). A minor increase in Paxalisib AUC (1.63-fold) was observed in combination.
c. Mirdametinib mean and standard deviation brain concentration-time profiles alone (mir) and in combination with Paxalisib (mir+pax) with 3 individual mice per time point. Only the 2-hour time point is significantly higher for the combination (907 vs 498 ng/mL, two-way ANOVA with Time-Combination interaction on log-transformed concentrations, Tukey HSD p=0.0001394)
d. Paxalisib mean and standard deviation brain concentration-time profiles alone (pax) and in combination (pax+mir) with 3 individual mice per time point. There are no significant differences between the groups for any time point at the a=0.05 level (two-way ANOVA with Time-Combination interaction on log-transformed concentrations).

   The error bars indicate the mean +/- SD.

Supplementary Fig 10: Pharmacokinetic (PK) analyses of Paxalisib and Mirdametinib show a lack of appreciable plasma or brain drug interaction and show high brain exposure

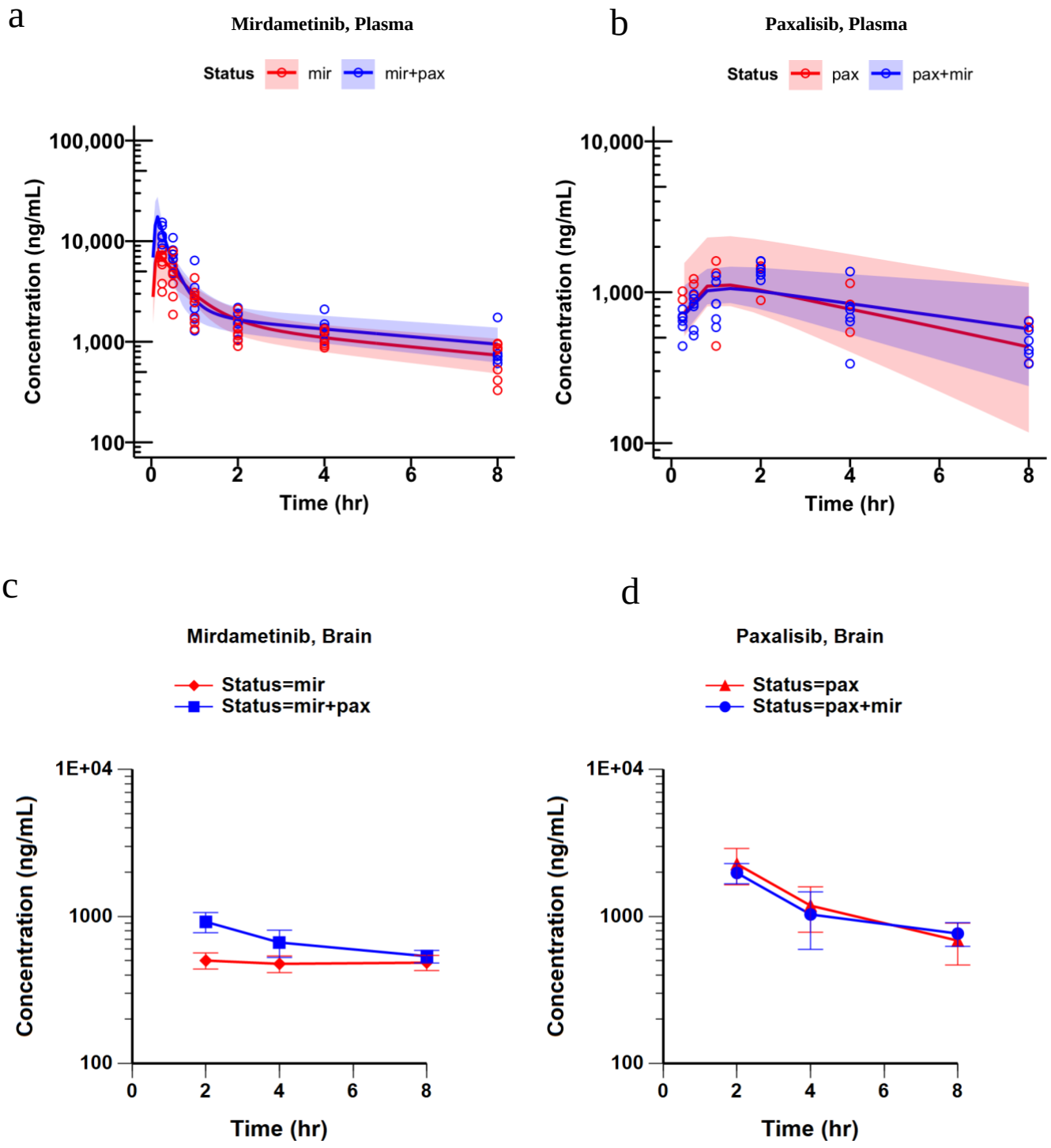

SUPPLEMENTARY TABLES

Supplementary Table 1: Cell line models used in HTS

Cell Line Name	Histone mutation status	Doubling-time 384W (coated) (days)	Seeding number (thousand)	PDOX Methylation Classification	Signature Mutations
SJ-HGGX2c	Wild-type	8.2	8	Glioblastoma, IDH wildtype, subclass midline	TP53, PDGFRA, PIK3R1, MET
SJ-HGGX39c	Wild-type	3.7	4	Glioblastoma, IDH wildtype, subclass RTK III	TP53, BCOR, CDKN2A, PDGFRA
SJ-HGGX6c	H3.3G34R	5.6	8	Glioblastoma, IDH wildtype, H3.3 G34 mutant	H3F3A (H3.3 G34R), PDGFRA, TP53, HIST2H3D, ATRX
SJ-HGGX42c	H3.3G34R	6.1	8	Glioblastoma, IDH wildtype, H3.3 G34 mutant	H3F3A (H3.3 G34R), TP53, ATRX, BCOR, PDGFRA, BRAF, CCND2
SJ-DIPGX7c	H3.3K27M	6.1	8	Diffuse midline glioma, H3 K27M mutant	H3F3A (H3.3 K27M), BCOR, TP53, PIK3CA
SJ-DIPGX9c	H3.1K27M	9.1	8	Diffuse midline glioma, H3 K27M mutant	HIST1H3B (H3.1 K27M), ACVR1, PIK3CA
SJ-DIPGX29c	H3.3K27M	9.0	8	Diffuse midline glioma, H3 K27M mutant	H3F3A (H3.3 K27M), TP53, CCND3
SJ-DIPGX37c	H3.3K27M	9.0	8	Diffuse midline glioma, H3 K27M mutant	H3F3A (H3.3 K27M), PIK3R1, PPM1D, NTRK1, PIK3CA
SU-DIPG-IV	H3.1K27M	3.0	8	Diffuse midline glioma, H3 K27M mutant	HIST1H3B (H3.1 K27M), MDM4, ACVR1
SU-DIPG-VI	H3.3K27M	5.8	8	Diffuse midline glioma, H3 K27M mutant	H3F3A (H3.3 K27M), TP53
SU-DIPG-XIII	H3.3K27M	6.6	8	Diffuse midline glioma, H3 K27M mutant	H3F3A (H3.3 K27M)
SU-DIPG-XVII	H3.3K27M	5.8	4	Diffuse midline glioma, H3 K27M mutant	H3F3A (H3.3 K27M)
SUDIPG-XIX	H3.3K27M	4.6	8	Diffuse midline glioma, H3 K27M mutant	H3F3A (H3.3 K27M)
SU-DIPG-XXI[1]	H3.1K27M	4.6	8	Diffuse midline glioma, H3 K27M mutant	HIST1H3B (H3.1 K27M)
iAstro	Wild-type	2.8	4	Not a PDOX	None
HA-bs	Wild-type	11.3	8	Not a PDOX	None
hNSC	Wild-type	2.6	4	Not a PDOX	None

Supplementary Table 2: Resource table of all reagents used for this study

Supplementary Table 2: Resource Table includes all reagents used for this study

HyClone™ Phosphate Buffered Saline (PBS)	Fisher Scientific, SH3025601
Paraformaldehyde, EM Grade	Electron Microscopy Sciences, 19200
Hematoxylin	Fisher Scientific, 7221
Eosin	Fisher Scientific, 7111
Anti-mouse biotinylated secondary antibodies	Vector Laboratories, BA-2000
Anti-rabbit biotinylated secondary antibodies	Vector Laboratories, BA-1000
Horseradish-peroxidase-conjugated streptavidin VECTASTAIN Elite ABC Kit	Vector Laboratories, PK-6100
DAB substrates	Vector Laboratories, SK-4100
Hematoxylin (for counter staining).	Vector Laboratories, H-3401
RIPA Buffer (10×)	Cell Signaling, 9806
cOmplete™ Protease Inhibitor Cocktail	Sigma-Aldrich, 11697498001
PhosSTOP™	Sigma-Aldrich, 4906845001
Micro BCA™ Protein Assay Kit	ThermoFisher, 23235
NuPAGE MES SDS Running Buffer (20×)	ThermoFisher, NP0002
NuPAGE™ 12%, Bis-Tris, 1.0 mm, Mini Protein Gel	ThermoFisher, NP0341PK2
NuPAGE™ Transfer Buffer (20×)	ThermoFisher, NP00061
NuPAGE™ Sample Reducing Agent (10×)	ThermoFisher, NP0004
NuPAGE™ LDS Sample Buffer (4×)	ThermoFisher, NP0007
NuPAGE™ 4 to 12%, Bis-Tris, 1.0 mm, Midi Protein Gel	ThermoFisher, WG1403BOX
Restore™ PLUS Western Blot Stripping Buffer	ThermoFisher, 46430
Pierce™ 20× TBS Buffer	ThermoFisher, 28358
TWEEN® 20	Bio-Rad, 1706531
Rabbit IgG HRP Linked Whole Ab (from Donkey)	MilliporeSigma GENA934-100UL
Mouse IgG HRP Linked Whole Ab Cytiva, NXA931	MilliporeSigma GENXA931-1ML
Amersham™ ECL™ Rainbow™ Marker - Full range	MilliporeSigma GERPN800E
SuperSignal™ West Dura Extended Duration Substrate	ThermoFisher 34075
Nitrocellulose/Filter Paper Sandwiches, 0.2 µm, 8.5 x 13.5 cm	ThermoFisher LC2009
Akt Antibody Rabbit pAb (1:1000 Western)	Cell Signaling, 9272
Phospho-Akt (Ser473) Antibody Rabbit pAb (1:50 IHC and 1:1000 Western)	Cell Signaling, 9271
p44/42 MAPK (Erk1/2) Antibody Rabbit (1:1000 IHC and Western)	Cell Signaling, 9102

Phospho-p44/42 MAPK (Erk1/2) (Thr202/Tyr204) Antibody Rabbit (1:1000 IHC and Western)	Cell Signaling, 9101
Phospho-Histone H3 (Ser10) Antibody (1:200 IHC)	Cell Signaling, 9701
Cleaved Caspase-3 Antibody Rabbit mAb (1:500 IHC)	BD, #559565
Anti-Nuclei Antibody, clone 235-1 (1:100 IF)	Millipore, MAB1281
Anti-Mitochondria Antibody, surface of intact mitochondria, clone 113-1 (1:50 IF)	Millipore, MAB1273
Mouse Cell Depletion Kit	Miltenyi Biotec, 130-104-694
KnockOut™ DMEM/F-12	ThermoFisher, 12660012
Neurobasal® Medium, minus phenol red	ThermoFisher, 12348017
B-27® Supplement, minus vitamin A	ThermoFisher, 12587010
N-2 Supplement	ThermoFisher, 17502048
StemPro® Neural Supplement	ThermoFisher, A1050801
Recombinant Human EGF	Peprotech, AF-100-15
Recombinant Human FGF-b	Peprotech, 100-18B
Recombinant Human PDGF-AA	Cell Guidance Systems, GFH16AF-100
Recombinant Human PDGF-BB	Cell Guidance Systems, GFH18AF-100
0.2% Heparin Sodium Salt in PBS	StemCell, 07980
Sodium Pyruvate (100 mM)	ThermoFisher, 11360070
MEM Non-Essential Amino Acids Solution (NEAA)	ThermoFisher, 11140050
GlutaMAX™ Supplement	ThermoFisher, 35050061
Bovine Albumin Fraction V (7.5% solution)	ThermoFisher, 15260037
Penicillin-Streptomycin (10,000 U/mL)	ThermoFisher, 15140122
DMEM/F-12, HEPES	ThermoFisher, 11330032
ACCUTASE™ cell detachment solution	Innovative Cell Technologies, Inc., AT 104
Accumax™ cell detachment solution	Innovative Cell Technologies, Inc., AM 105
HEPES (1M)	ThermoFisher, 15630080
Geltrex™ LDEV-Free, hESC-Qualified	ThermoFisher, A1413302
Corning™ Matrigel™ hESC-Qualified Matrix	FisherScientific,08-774-552 Corning™, 354277
Primocin	Invivogen, ant-pm-1
ENStem-A™ Neural Freezing Medium (1X)	EMDMillipore, SCM011
STEMdiff™ Neural Progenitor Freezing Medium	StemCell, 05838
Cell Freezing Medium-DMSO 1×	MilliporeSigma, C6295
NeuroCult™ Proliferation Kit (Mouse & Rat)	StemCell, 05702
Corning® 384-well Flat Clear Bottom White Polystyrene TC-treated Microplates	Corning, 3765
BrandTech, 384-well pureGradeTM S	BrandTech, 781686
Corning® 96-well polypropylene deep well V-bottom	Corning, 3960

Corning® Ultra-Low Attachment 25cm² Rectangular Canted Neck Cell Culture Flask with Vent Cap	Corning, 3815
Corning® Ultra-Low Attachment 75cm² U-Flask Canted Neck Cell Culture Flask with Vent Cap	Corning, 3814
Corning® 75cm² U-Shaped Canted Neck Cell Culture Flask with Vent Cap	Corning, 430641U
Corning® 175cm² U-Shaped Angled Neck Cell Culture Flask with Vent Cap	Corning, 431080
Falcon™ Cell Strainers	FisherScientific, 08-771-1
MACS SmartStrainers (30 µm)	Miltenyi Biotec, 130-098-458
MidiMACS™ Separator and Starting Kits	Miltenyi Biotec, 130-090-329
LS Columns	Miltenyi Biotec, 130-042-401
Papain	Worthington, LS003126
N-Acetyl-L-cysteine (NAC)	Sigma-Aldrich, A9165
DNase I, from bovine pancreas	Sigma-Aldrich, 11284932001
D-Luciferin, Firefly	PerkinElmer, 122799
CellTiter-Glo® Luminescent Cell Viability Assay	Promega, G7573
Methyl cellulose	Sigma-Aldrich, M7027
TWEEN® 80	Sigma-Aldrich, P4780
Distilled Water for formulation	ThermoFisher, 15230147
Human iPSC-derived astrocytes, Tempo-iAstro™	Tempo Bioscience®
Human Astrocytes-brain stem, HA-bs	ScienCell Research Laboratories, 1840
GIBCO® Human Neural Stem Cells (H9 hESC-Derived)	Invitrogen, N7800-100
GDC-0084	Chemgood (company ID#C-11-41), CAS#1382979-94-3
PD-0325901	Chemietek (Lot#03), CAS# 391210-10-9

Supplementary Table 3: Primer sequences

Primer Names	Sequence	Amplicon size (bp)
Human *H3F3A*-F	GTA AAA CGA CGG CCA GTG ATT TTG GGT AGA CGT AAT CTT CA	450
Human *H3F3A*-R	CAG GAA ACA GCT ATG ACC TTT CCT GTT ATC CAT CTT TTT GTT	450
Mouse *h3f3A*-F	AGA CAC TAT CCC ACT GCT CGA CG	442
Mouse *h3h3A*-R	GGG GCG TCT CTC TGG TTT TGG C	442

Supplementary Note 1

Detailed information for drug-drug interaction pharmacokinetic study of mirdametinib and paxalisib in non-tumor bearing female CD-1 nude mice

In Vivo Pharmacokinetic (PK) Study Design

The plasma pharmacokinetics (PK) of the MEK inhibitor mirdametinib (PD-0325901) and PI3K inhibitor paxalisib (GDC-0084) were studied to determine whether a PK drug-drug interaction (DDI) exists between these agents when co-administered orally in mice. A moderate interaction, defined as a ≥2-fold difference in plasma area under the concentration-time curve (AUC) or apparent oral clearance (CL/F), was considered as impactful and practically significant.

In the main study (Study 1), 3 groups of 9 mice each were studied with a mixed, staggered survival and terminal sampling design. Mirdametinib (Chemietech, CT-PD03, Lot# 3) and paxalisib (Chemgood, C-1141) were each suspended in 1% methylcellulose (type 400 cPs) / 1% Tween 80, with the combination co-formulated and administered as a single 10 mL/kg gavage. On Day 1, mice received single 5 mL/kg oral doses of each drug alone, with 2 retro-orbital blood samples obtained under isoflurane anesthesia, up to 8 hours post-dose. For the next 4 days, mice received daily (i.e. every 24 ± 2 hours) combination therapy or mirdametinib monotherapy. On Day 5, another PK study was performed following combination or mirdametinib monotherapy, with one survival and terminal blood sample acquired per mouse.

Paxalisib PK was also assessed in a similar combination PK DDI study with another targeted anti-cancer agent DrugX (Study 2). On Day 1, paxalisib single agent PK was studied. Then for the next 4 days, mice received daily combination therapy with DrugX or paxalisib monotherapy, with combination or single agent PK evaluated on Day 5, respectively.

For survival samples, blood from the retro-orbital plexus, 50 -100 µL, was collected into Sarstedt Minivette POCT KEDTA capillary devices. Plasma was immediately isolated and placed on dry ice until transfer to -80 °C for storage. At the terminal time points, blood was collected via cardiac puncture into a Sarstedt Microvette 500 KEDTA microtube, mice were perfused with PBS, and the brains extracted. All plasma and brain samples were stored on dry ice and transferred to -80 °C at the end of study. An outline of the studies and groups are presented in Supplementary Data 5a.

Bioanalysis

Plasma and brain homogenate (Dilution Factor = 6, with ultrapure water) were subjected to deproteinization and analyzed for mirdametinib and paxalisib concentrations using a qualified LC-MS/MS assay with loperamide as the internal standard. Stock and spiking solutions were prepared in methanol and used to spike matrix calibrators and quality controls. Matrix samples, 25 µL each, plus 25 µL of IS (5 ng/mL in methanol) were protein precipitated with 100 µL of acetonitrile. A 5 µL aliquot of the supernatant was injected onto a Shimadzu LC-20ADXR high performance liquid chromatography system via a Shimadzu SIL-20AC XR autosampler. The LC separation was performed using a Phenomenex Kinetex C18 (2.6 µm, 50 mm x 2.1 mm) column at 40˚C with gradient elution at a flow rate of 0.25 mL/min. The binary mobile phase consisted of 0.2% formic acid in methanol: water (10:90, v/v) in reservoir A and 0.2% formic acid in methanol in reservoir B. The initial mobile phase composition was maintained at 10% B for 0.5 minutes and was followed by a linear increase to 100% B in 2.5 minutes. The column was then rinsed for 1 minute at 100% B and then equilibrated at the initial conditions for 2 minutes for a total run time of 6 minutes. Under these conditions, mirdametinib eluded at 3.31 minutes, paxalisib at 3.00 minutes, and IS at 3.16 minutes. Analytes and IS were detected with tandem mass spectrometry using a SCIEX API 4000 in the positive ESI mode with the following mass were transitions monitored: mirdametinib 482.90 -> 249.00, paxalisib 383.30 -> 353.20, and loperamide 477.30 -> 266.10.

The method qualification and bioanalytical runs all passed acceptance criteria for non-GLP assay performance. A linear model ($1/X^2$ weighting) fit the calibrators across the 1 to 100 ng/mL range, with a correlation coefficient (R) of ≥0.9959. Sample dilution integrity was confirmed. The lower limit of quantitation (LLOQ), defined as a peak area signal-to-noise ratio of 5 or greater verses a matrix blank with IS, was 1 ng/mL for plasma and 6 ng/mL for brain homogenate secondary to the dilution. The intra-run precision and accuracy was ≤ 7.36% CV and 88.2% to 113%, respectively.

Pharmacokinetic (PK) Analysis

Summary statistics for mirdametinib and paxalisib concentration-time (Ct) data in plasma and brain were generated by study, occasion (Day 1 vs. Day 5), combination status, and nominal time point and presented in tabular form, along with Mean (SD) Ct profile figures, using Phoenix WinNonlin 8.1 (Certara USA, Inc., Princeton, NJ).

Plasma Ct data for mirdametinib and paxalisib were grouped by study, analyte, individual mouse, occasion, and combination status and analyzed using nonlinear mixed effect (NLME) modeling implemented in Monolix 2019R2 (Lixoft SAS, Antony, France). Parameters and the Fisher Information Matrix (FIM) were estimated using the stochastic approximation expectation maximization (SAEM) algorithm, and the final log-likelihood estimated with importance sampling, all using the default Monolix initial settings. A variety of models were fit to the Ct data, parameterized using apparent clearances or rate constants, volumes of distribution, and absorption rates as needed. These models were assessed for goodness of fit using the -2 log likelihood (-2LL) value, Akaike and Bayesian Information Criterion (AIC, BIC), visual predictive checks, plots of model individual and population predicted vs. observed data, residual plots, and the standard errors of parameter estimates. A log-normal inter-individual (omega) and inter-occasion (gamma) distribution was assumed on selected supported parameters, with only diagonal elements of parameter covariance matrices estimated. Additive and/or proportional residual error

models were tested and implemented as supported. Beal's M3 method was used to handle any data that were below the LLOQ[1].

The compound combinations were tested as categorical covariates upon the mirdametinib or paxalisib supported PK parameters, primarily the apparent oral clearance (CL/F). The covariate effect was considered statistically significant if its addition reduced the -2LL by at least 3.84 units ($P < 0.05$, based on the χ^2 test for the difference in the -2LL between two hierarchical models that differ by 1 degree of freedom). Additionally, Wald test P values were outputted for the interaction covariate effect levels by the software, and reported in the Results tables. Secondary PK parameters such as the maximum concentration (Cmax), time of Cmax (Tmax), area under the Ct curve (AUC), and apparent terminal half-life (T1/2) were derived from the model parameter estimates using standard formulae for the relevant compartmental model[2].

Mirdametinib Pharmacokinetics in Mice

The plasma PK of mirdametinib was well-described using a linear, two-compartment model with zero-order absorption. Absorption was rapid, with the Tmax generally occurring at the 0.25 hr time point. As there was no observable data in the absorption phase, the zero-order absorption rate (Tk0) was fixed to 0.125 hr. The plasma Ct profile showed a distribution phase lasting approximately 1 hr, followed by an apparent terminal phase with a half-life of ~ 4 hrs. No accumulation occurred with daily dosing for 5 days in mice. Apparent oral clearance (CL/F) was low at 12.9 mL/min/kg or ~14% of hepatic blood flow. The apparent volume of distribution was large and greater than total body water. The bioavailability of mirdametinib was not evaluated in this study, but has previously been reported to be ~30% in rats (data not shown).

A linear two-compartment model with inter-individual and inter-occasion variability on both apparent oral clearance (CL/F) and apparent oral volume of distribution (Vc/F), and proportional residual error best described the overall plasma Ct data. The precision of the

variability estimates was poor likely due to model overparameterization and the small number of mice and samples available; however, the goodness of fit plots and post hoc individual visual predictive checks indicated adequate performance. Combination status was tested as a covariate on CL/F and Vc/F inter-occasion variability, and its addition on both parameters improved the model fit (-2LL P=0.0003714858), indicating a statistically significant effect of paxalisib co-administration on mirdametinib plasma PK.

There was a 23.1% reduction in mirdametinib CL/F with combination therapy (P=0.0124957), and a 61.9% decrease in Vc/F (P=0.000159031). This resulted in a 2.63-fold higher Cmax, but only a 1.30-fold increase in AUC. Therefore, no practical effect of paxalisib upon mirdametinib PK by the predefined ≥2-fold difference of AUC or CL/F criteria was observed. This lack of a practical effect is supported by comparison of Ct plots. The parameter estimates from the full mirdametinib model are presented in Supplementary Data 5b with the model predicted median, 90% prediction interval, and observed plasma mirdametinib concentrations presented in Supplementary Fig. 10a.

Paxalisib Pharmacokinetics in Mice

The plasma PK of paxalisib was well-described using a linear, one-compartment model with first-order absorption. Absorption rate was moderate and showed low-to-moderate variability, with the Tmax occurring at 1-2 hrs post-dose. The absorption rate appeared slower on Day 5 in combination vs. Day 1. The plasma Ct profile appeared monophasic, showing a terminal phase half-life ranging from 4.47 hrs alone to 7.28 hrs with mirdametinib. Significant accumulation occurred with daily dosing for 5 days in mice. Apparent oral clearance (CL/F) was low-to-moderate at 19.3 mL/min/kg or ~21.5% of hepatic blood flow. The apparent volume of distribution was large and greater than total body water. The bioavailability of paxalisib was not evaluated in this study, but has been reported to be high in various preclinical species.

A linear one-compartment model with inter-individual variability on first-order absorption rate (ka), apparent oral clearance (CL/F), apparent oral volume of distribution (Vc/F), and inter-occasion variability on apparent oral clearance (CL/F), and proportional residual error best described the overall plasma Ct data. The precision of some variability estimates was poor likely due to model overparameterization; however, the goodness of fit plots and post hoc individual visual predictive checks indicated adequate performance.

Combination status was tested as a covariate on CL/F inter-occasion variability, and its addition significantly improved the model fit (-2LL P=0.0005042182), suggesting a statistically significant effect of either mirdametinib and/or DrugX co-administration or study day on paxalisib plasma PK.

There was a 38.6% reduction in paxalisib CL/F in combination with mirdametinib on Day 5 (P=0.000218137), resulting in a statistically significant 1.63-fold increase in paxalisib AUC. This failed to meet the ≥2-fold difference of AUC or CL/F criteria, and therefore we conclude that there is no practical effect of mirdametinib upon paxalisib PK. This is also supported visually by comparison of Ct plots. The parameter estimates from the full paxalisib model are presented in Supplementary Data 5c with the model predicted median, 90% prediction interval, and observed plasma paxalisib concentrations presented in Supplementary Fig. 10b.

Pharmacokinetic summary

The plasma PK of mirdametinib 14 mg/kg PO in mice is similar to that previously reported with respect to the Ct curve shape. However, the AUC increased less than proportionally compared with clinically relevant doses of 0.5 and 1.5 mg/kg PO[3], suggesting saturable absorption, lower bioavailability, or higher clearance in our mice at the 14 mg/kg dose. Mirdametinib plasma PK after multiple doses appeared similar (Day 1 vs Day 5), suggesting it has time-invariant PK in mice. While a higher mirdametinib plasma Cmax was observed

in combination, the AUCs were not practically different (1.30-fold) – as this failed to meet the ≥2-fold criteria, paxalisib has no practical effect upon mirdametinib PK in mice. The brain penetration of mirdametinib appeared similar alone and in combination on Day 5 (Kp,last 0.502 and 0.524, respectively), and similar to published data in mice[4]. The plasma PK of paxalisib 8 and 10 mg/kg PO in mice, after a single dose on Day 1, is similar to that reported at 25 mg/kg, assuming dose proportional PK[5].

The brain penetration of paxalisib on Day 5 in combination (Kp,last = 1.42) was similar to that reported previously (single dose Kp,6hr = 1.39)[5]. There was no difference in paxalisib brain concentration either alone or in combination with mirdametinib or DrugX. Paxalisib's plasma AUC was 1.63-fold higher than expected in combination with mirdametinib. While this difference was statistically significant, indicating a possible weak drug interaction, it failed to meet the ≥2-fold critera for a practical interaction. Therefore mirdametinib had no practical effect on the PK properties of paxalisib.

Mirdametinib and paxalisib total plasma AUCs at these dose levels in mice exceed those observed clinically in humans. A PK-guided clinically relevant dose for mirdametinib, equivalent to 4 mg PO BID in humans[6], would be 0.5 mg/kg PO BID in mice. Likewise for paxalisib, a PK-guided dose similar to 45 mg PO QD in humans[7] would be approximately 2 mg/kg to 4.5 mg/kg PO QD in mice.

References for Supplementary Note 1

1 Beal, S. L. Ways to fit a PK model with some data below the quantification limit. *J Pharmacokinet Pharmacodyn* **28**, 481-504, doi:10.1023/a:1012299115260 (2001).

2 Gibaldi, M. & Perrier, D. *Pharmacokinetics, Second Edition*. (CRC Press, 1982).

3 Jousma, E. *et al.* Preclinical assessments of the MEK inhibitor PD-0325901 in a mouse model of Neurofibromatosis type 1. *Pediatr Blood Cancer* **62**, 1709-1716, doi:10.1002/pbc.25546 (2015).

4 de Gooijer, M. C. *et al.* The impact of P-glycoprotein and breast cancer resistance protein on the brain pharmacokinetics and pharmacodynamics of a panel of MEK inhibitors. *International journal of cancer* **142**, 381-391, doi:10.1002/ijc.31052 (2018).

5 Salphati, L. *et al.* Brain Distribution and Efficacy of the Brain Penetrant PI3K Inhibitor GDC-0084 in Orthotopic Mouse Models of Human Glioblastoma. *Drug metabolism and disposition: the biological fate of chemicals* **44**, 1881-1889, doi:10.1124/dmd.116.071423 (2016).

6 LoRusso, P. M. *et al.* Phase I pharmacokinetic and pharmacodynamic study of the oral MAPK/ERK kinase inhibitor PD-0325901 in patients with advanced cancers. *Clinical cancer research : an official journal of the American Association for Cancer Research* **16**, 1924-1937, doi:10.1158/1078-0432.CCR-09-1883 (2010).

7 Wen, P. Y. *et al.* A first-in-human phase 1 study to evaluate the brain-penetrant PI3K/mTOR inhibitor GDC-0084 in patients with progressive or recurrent high-grade glioma. *Journal of Clinical Oncology* **34**, 2012-2012, doi:10.1200/JCO.2016.34.15_suppl.2012 (2016).